Supporting information for

Enhanced Conformational Sampling Using Replica Exchange with Concurrent Solute Scaling and Hamiltonian Biasing Realized in One Dimension

Mingjun Yang, Jing Huang and *Alexander D. MacKerell, Jr.*[a)]

Department of Pharmaceutical Sciences, School of Pharmacy, University of Maryland, Baltimore, Maryland 21201

a) To whom correspondence should be addressed: alex@outerbanks.umaryland.edu

Table S1. Parameter distribution and acceptance ratios (AR) in the simulations of the M5 system

replica index	T / K	λ	[b]AR/HREST-BP	AR/REST2	[b]AR/H-REX
0	298	0.00	26.6%	38.7%	54.1%
1	322	0.13	29.1%	38.8%	53.8%
2	348	0.23	34.9%	40.2%	61.7%
3	376	0.28	39.3%	41.7%	67.4%
4	407	0.33	39.4%	42.9%	61.2%
5	440	0.39	40.0%	44.2%	58.3%
6	475	0.44	42.0%	45.1%	57.3%
7	514	0.49	42.1%	46.5%	50.7%
8	555	0.56	43.1%	47.9%	45.9%
9	600	0.64	44.5%	48.7%	45.4%
[a]AAR			38.1%	43.5%	55.1%

a) AAR– the average acceptance ratio over all 10 replicas with a simulation time of 20 ns for each replica.
b) The biasing potentials used are marked in Figure 1b.

Table S2. Parameter distribution and acceptance ratios (AR) in the simulations of the *1→6* linked disaccharide

replica index	T / K	λ	[b]AR/HREST-BP	AR/REST2	[b]AR/H-REX
0	298	0.00	30.9%	33.5%	79.7%
1	342	0.17	29.5%	34.5%	73.9%
2	392	0.36	28.2%	35.6%	64.4%
3	450	0.51	28.3%	35.7%	60.7%
[a]AAR			29.2%	34.8%	69.7%

a) AAR– the average acceptance ratio over all 4 replicas with a simulation time of 20 ns for each replica.
b) The biasing potentials used are marked in Figure 1c.

Table S3. Parameter distribution and acceptance ratios (AR) in the simulations of the *1→4* linked disaccharide

replica index	T / K	λ	AR/HREST-BP[b]	λ	AR/HREST-BP[c]
0	298	0.00	49.4%	0.00	35.2%
1	327	0.17	38.3%	0.21	24.3%
2	373	0.54	28.0%	0.52	20.6%
3	429	0.71	28.2%	0.67	26.0%
4	496	0.87	35.6%	0.84	32.8%
5	553	1.04	43.2%	1.00	41.0%
[a]AAR			37.1%		30.0%

a) AAR– the average acceptance ratio over all 6 replicas with a simulation time of 20 ns for each replica.
b) Only the 2D bpCMAP was used along the linkage dihedrals φ1/ψ1 in this HREST-BP simulation (see Figure 1d in main text).
c) The 2D bpCMAP along the linkage dihedrals φ1/ψ1 and 1D biasing potential about ϕ2, ω2 and ω3 were used in this HREST-BP simulation (see Figure 1d in main text).

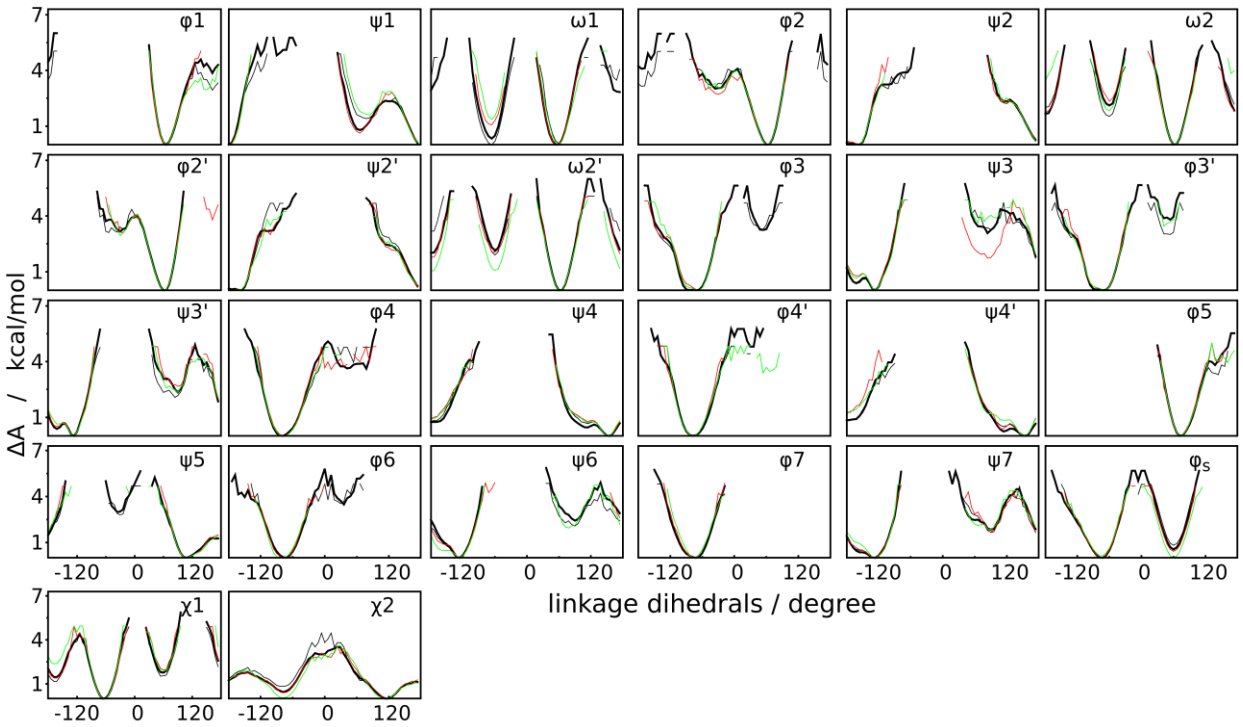

Figure S1. Free energy profiles along the linkage dihedrals of SCT in the simulation with HREST-BP (black), H-REX (green) and REST2 (red), which were computed from the first 20 ns of the ground-state trajectory (thin lines). The bold black line shows the result from the 100 ns ground-state trajectory in the HREST-BP simulations. These results show the convergence of localized motions along the glycosidic linkages to occur within a simulation time of 20 ns.

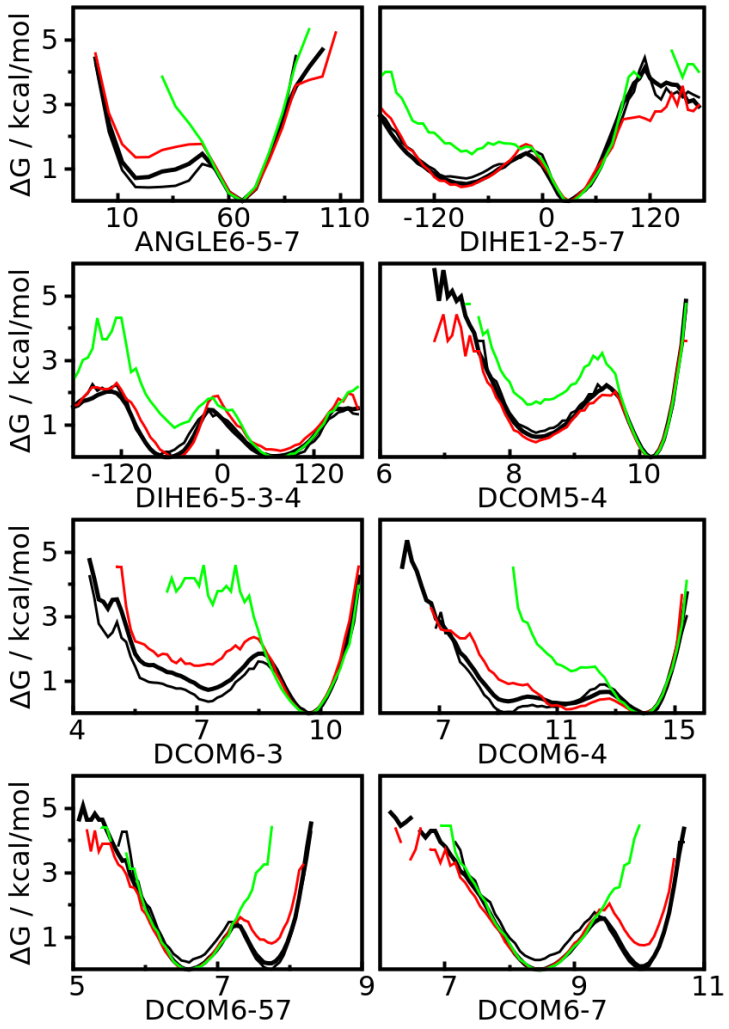

Figure S2. Free energy profiles along the pseudo-angles (in degree), dihedrals (in degree), and distances (in Å) defined using the center of mass (COM) of different sugar rings in the simulations of M5 using HREST-BP (black), H-REX (green) and REST2 (red). The reference profiles were computed using a 90 ns HREST-BP simulation (in bold line) and thin lines show the results from 20 ns simulations. All the examined profiles with more than one local minima are shown in this figure. These results highlight the importance of the inclusion of Hamiltonian temperature scaling of the whole solute in sampling long-distance motions.

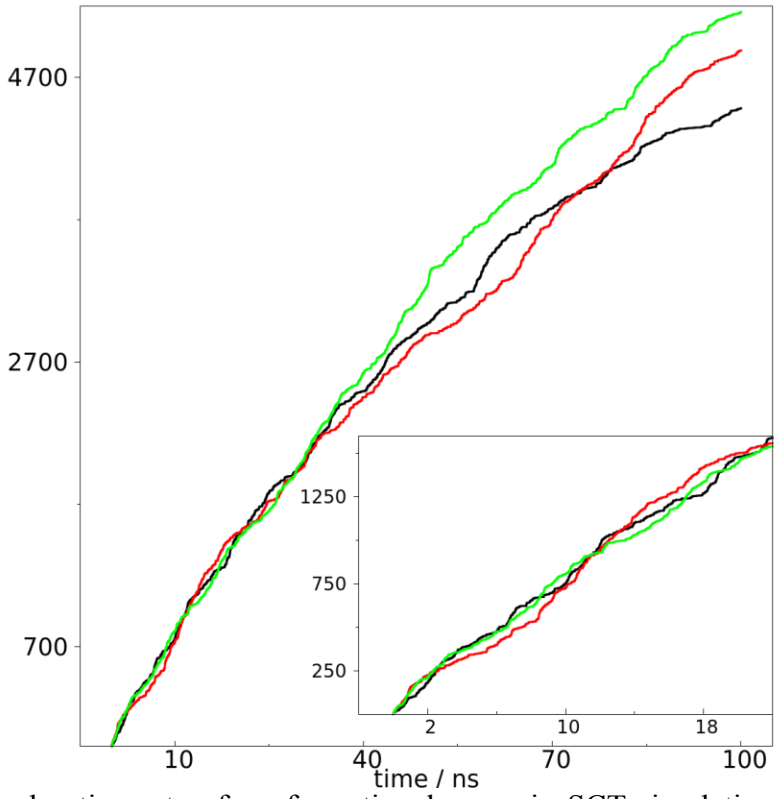

Figure S3. The exploration rate of conformational space in SCT simulations with HREST-BP (black), H-REX (green), and REST2 (red). Each dihedral was divided into three bins [0°, 120°], [-120°, 0°], and [-180°, -120°] & [120°, 180°], resulting in a total of 3^N states where N is the number of dihedrals marked in Figure 1 with more than one local minima. The exploration rate is defined as the number of visited conformations with different states at simulation time t. The inset highlights the result for the first 20 ns. The results suggest a comparable exploration rate for the 3 different simulation methods during the first 20 ns within which the statistically important local minima are converged (see Figure S1).

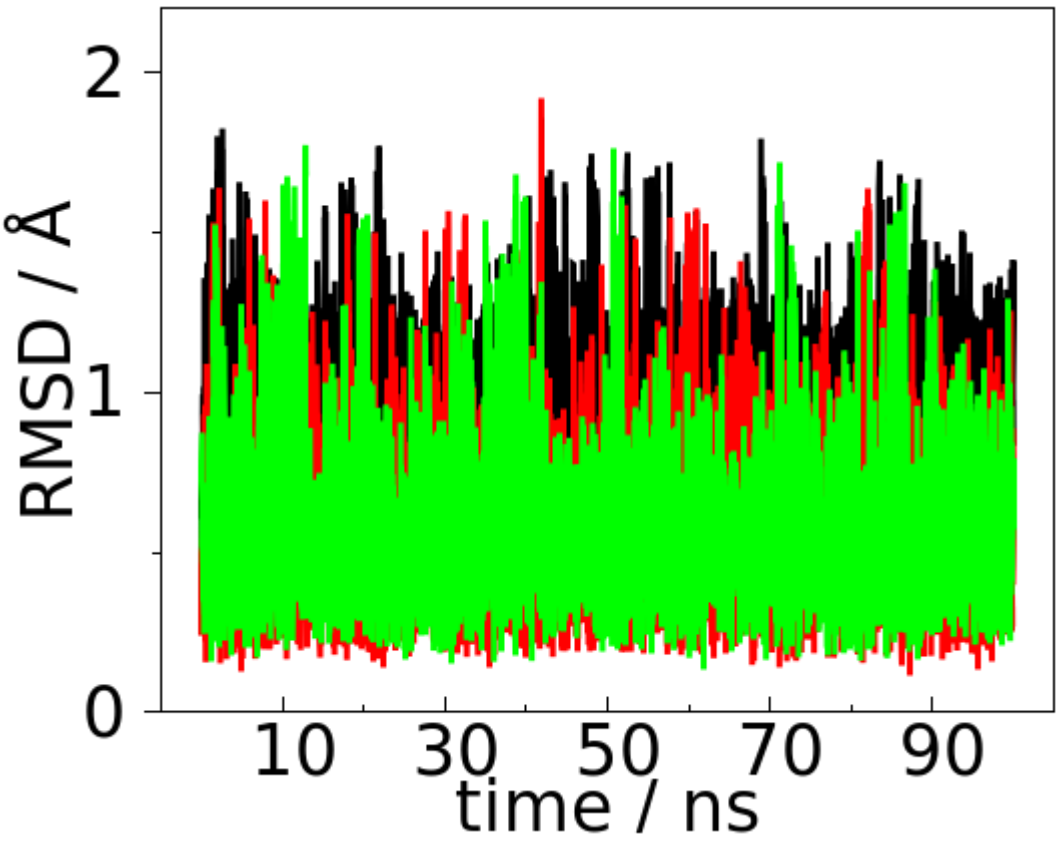

Figure S4. RMSD evolution in the ground-state replica of the HREST-BP simulation for three rigid fragments of SCT: black for -D-Man*p*(3)-β-(*1*→*4*)-D-Glc*p*NAc(2)-β-(*1*→*4*)-D-Glc*p*NAc(1)-β-1-, red for -D-Gal*p*(6)-β-(*1*→*4*)-D-Glc*p*NAc(5)-β-(*1*→*2*)-D-Man*p*(4)-α-1-, and green for -D-Gal*p*(10)-β-(*1*→*4*)-D-Glc*p*NAc(9)-β-(*1*→*2*)-D-Man*p*(8)-α-1-. Each fragment was aligned to the starting conformation and then the RMSD was computed for each snapshot based on the ring atoms. The small RMSD fluctuation suggests relatively small changes in the intramolecular geometries of three fragments.

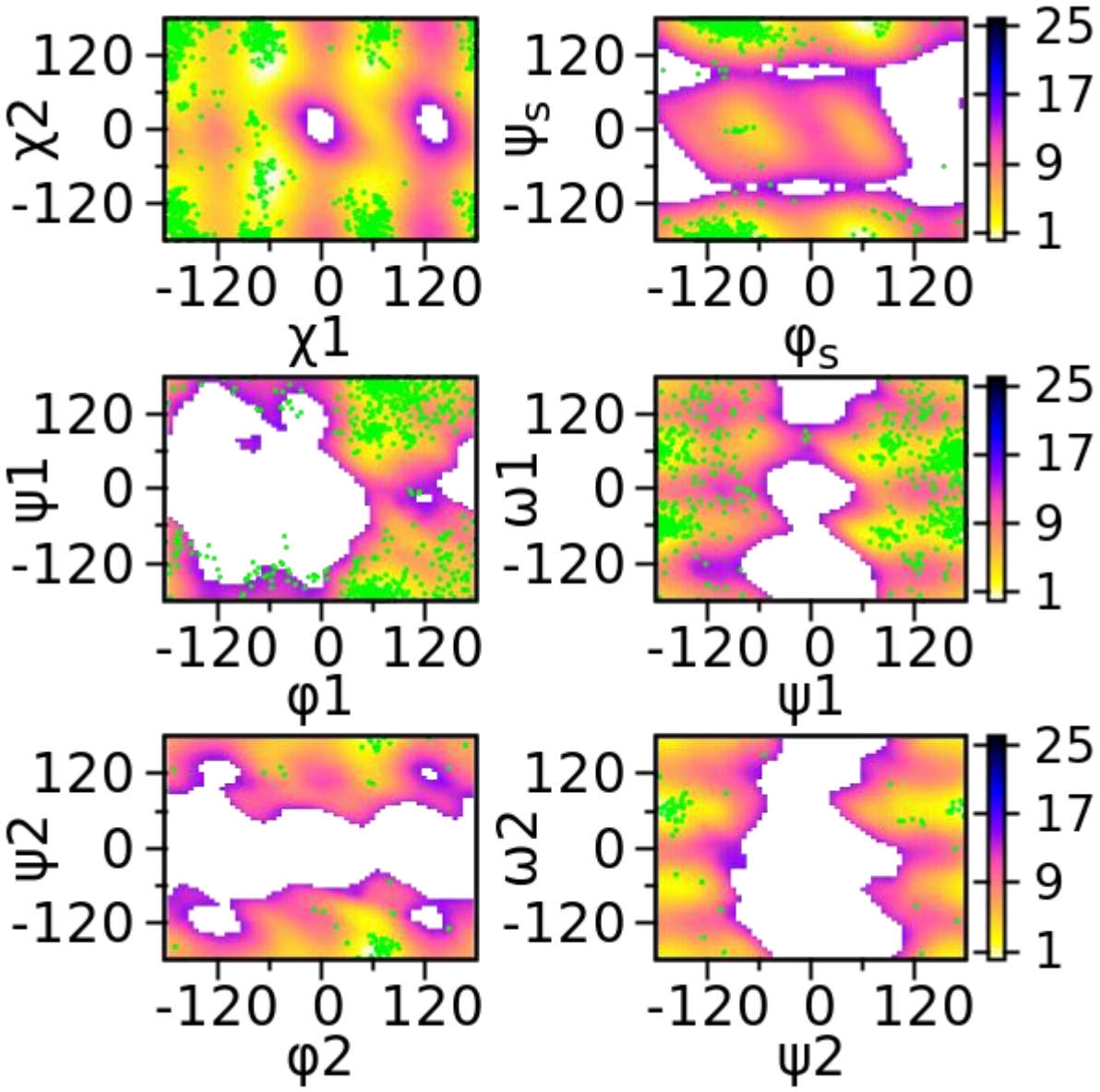

Figure S5. PMF maps from 2D umbrella sampling along the dihedrals in model compounds: D-Glc*p*NAc-β-1→Asn (top), D-Man*p*-α-(*1*→*6*)-D-Man*p*-β-1-OMe- disaccharide (middle), and D-Neu*p*5Ac-α-(*2*→*6*)-D-Gal*p*-β-1-OMe disaccharide. The green points are data from crystal surveys that include the corresponding model compounds.[1] These results suggest a reasonably accurate representation of these flexible linkages by the force field as the majority of clusters of crystal conformations correspond to the local minima of the model compounds.

References

1. Jo, S.; Im, W. *Nucleic Acids Res.* **2013,** *41* (D1), D470-D474.